Practical Application of the Whipple and Carvallo Stability Model on Modern Bicycles with Pedal Assistance

Sien Dieltiens [1],*, Frederik Debrouwere [2] , Marc Juwet [1] and Eric Demeester [3]

[1] KU Leuven Technologie Campus Gent, 9000 Gent, Belgium; marc.juwet@kuleuven.be
[2] KU Leuven Campus Brugge, 8200 Brugge, Belgium; frederik.debrouwere@kuleuven.be
[3] KU Leuven Campus Diepenbeek, 3590 Diepenbeek, Belgium; eric.demeester@kuleuven.be
* Correspondence: sien.dieltiens@kuleuven.be

check for
updates

Abstract: Increasingly more people cycle with electrically-powered pedal assistance. The reduced pedalling effort attracts physically challenged people and seniors, who have a higher risk of falling. Since electric bicycles are heavier and the centre of masses are located higher, accidents happen easily. This study analyses the influence of the addition of a battery and motor unit on the stability behaviour of common bicycles for women. Based on market research, seven typical bicycle configurations are determined. Geometrics, mass values, and cycling postures are measured, and the theoretical stability behaviour is determined analytically based on the stability model of Whipple and Carvallo. The research shows that bicycles without pedal assistance have a smaller self-stable and semi-stable range than most electric bicycles. The electric bicycle with a motor implemented in the front wheel perform best, as the extra weight of the motor enhances the gyroscopic self-stabilization of the front wheel. Furthermore, a battery in the lower mid-tube is preferred over one in the luggage rack as it lowers the center of mass of the rear frame assembly. Knowledge about the optimal configuration to maximize the stability will enhance the cycling comfort and minimize the chance of accidents.

Keywords: whipple; caravallo; self-stability; bicycle dynamics

1. Introduction

It is generally accepted that cycling is an easy and intuitive activity accessible for nearly all. Though, learning to cycle demands some bravery. Instinctively, newcomers pedal gently and cautiously, which results in a low speed and an unstable bicycle. Only when levelling up the speed, the bicycle becomes stable and easily manageable.

The stability behaviour of bicycles is subject to numerous research studies. In 1899, the initial equations were formulated by Carvallo and Whipple to correctly estimate the stability behaviour of a bicycle without a cyclist [1,2]. The Carvallo Whipple model formed the base of various, new adapted and expanded models, which are listed in a fairly complete review by Meijaard et al. [3]. Meijaard et al. compared and evaluated the wide variety of models theoretically, based on a benchmark bicycle. The models were, furthermore, evaluated experimentally by, e.g., Jones, Stevens, Weir, and Zellner [4–6].

Schwab et al. [7] created a generally accepted, accurate, and feasible method to theoretically calculate stability behaviour in the function of different bicycle dimensions and compositions [8].

Adding an electromotor or battery-unit to the model is, to the author's knowledge, never addressed in literature, even though increasingly more people cycle with electrically-powered pedal assistance [9]. The decreased pedalling effort attracts seniors and physically challenged people who have an increased chance of accidents [10]. According to Twisk et al., a higher centre of mass may destabilize a bicycle, which is the case for electric bicycles due to the addition of the battery-unit [11].

To maximize the stability of electric bicycles and minimalize the chance on accidents, this study analyses the influence of different motor and battery placements on the stability behaviour of conventional recreational bicycles. Singularly bicycles for women are addressed, as 80% of all sold electric bicycles considers no upper mid tube and are for recreational use. Fifty popular bicycles for women with and without pedal assistance are segmented into seven typical bicycle configurations. The mean geometrics, mass values, and cycling postures are defined. The theoretical stability behaviour is calculated based on Meijaard et al. [3] and Schwab et al. [7]. The results are compared and evaluated.

2. Materials and Methods

A comparison is made between the self-stable behaviour of bicycles for women with pedal assistance and bicycles for women without pedal assistance. The geometrics, mass values, and the cycling posture of 50 popular bicycles are measured and the self-stable range is calculated based on the Carvallo Whipple Model [1,2] with the reviewed work of Meijaard et al. [3].

2.1. Object

City bicycles for women with pedal assistance (referred to as electric bicycles) and without pedal assistance (referred to as conventional bicycles) form the object of the research. City bicycles are designed as safe and comfortable means of transportation for everyday use. They are equipped with suspension in the fork, lights, a bell, gears, a luggage rack, and mudguards. Speed is of little import. The cyclists adopt a relaxed posture situated between the 'Dutch bike position,' which is fully vertical with a high aerodynamic drag and the 'trekking bike position,' which has a bit more bent forward for a higher pedalling efficiency, which is presented in Figure 1.

| (**a**) | (**b**) | (**c**) | (**d**) |
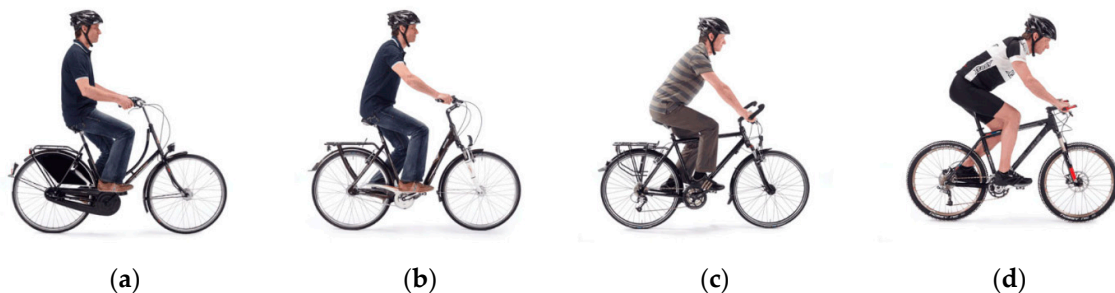
Figure 1. (**a**) Dutch bike position; (**b**) city bike position; (**c**) trekking bike position; (**d**) racing bike position.

Modern electric bicycles can be segmented into six categories, which distinguish themselves by motor placement and battery placement, as presented in Figure 2. The motor is located in the front wheel (electric bicycle 1, 2), rear wheel (electric bicycle 3, 4), or bottom bracket (electric bicycle 5, 6), and the battery is located in the luggage rack (electric bicycle 1, 3, 5) or lower mid-tube (electric bicycle 2, 4, 6).

| (**1**) | (**2**) | (**3**) | (**4**) | (**5**) | (**6**) |
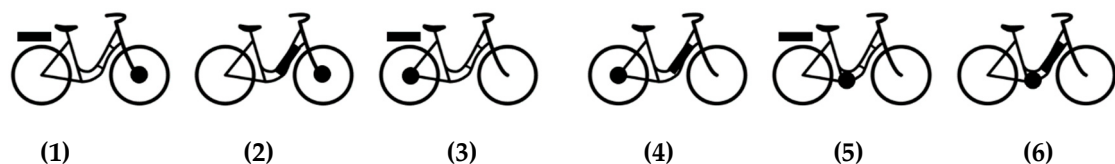
Figure 2. Electric bicycle configuration 1 till 6.

2.2. Model

The Carvallo Whipple model is utilized to determine the stability behaviour of a conventional bicycle and six electric bicycles [1,2]. The model considers four rigid bodies to embody a bicycle: a front wheel (F), a front frame including a fork and handlebar (H), a rear wheel (R), and a rear frame

including a rigidly attached rider (B), as seen in Figure 3. The model ignores motion of the rider relative to the frame, joint friction, structural compliances, and dampers.
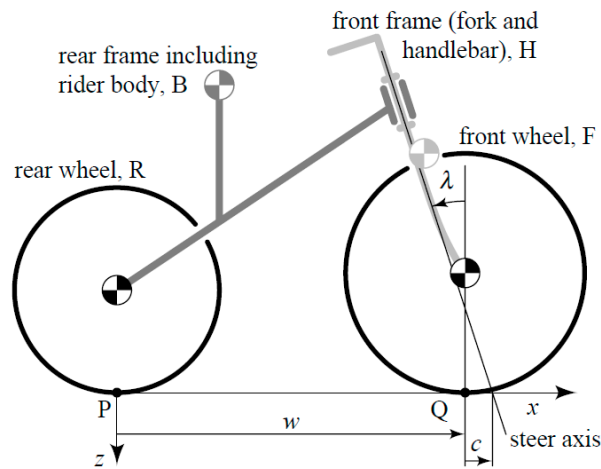

Figure 3. The four rigid bodies of a bicycle.

The longitudinal motion of the bicycle can be described by a single degree of freedom when an ideal contact is assumed between the rigid wheels and road surface with knife-edge rims and without longitudinal tire slip. The rear wheel rotates with θ_R relative to the rear frame (with forward motion being negative). The lateral motion of the bicycle can be described by two degrees of freedom when the lateral tire slip is assumed to be zero: the steer angle is δ (with right steering being positive) and the lean is ϕ (with right leaning being positive). When the bicycle is moving at a constant forward speed, the linearized equation of the Carvallo Whipple model for the lateral motion is given by Equation (1).

$$M\ddot{q} + vC_1\dot{q} + \left(v^2 K_2 + g K_0\right)q = f \tag{1}$$

where $q = [\phi, \delta]^T$ is the vector of degrees of freedom, $f = \left[T_\phi, T_\delta\right]$ is the vector of applied generalised forces, vC_1 is the non-symmetric velocity sensitivity matrix, and $v^2 K_2 + g K_0$ is the non-symmetric stiffness matrix. M, C_1, K_0 and K_2 are defined in terms of 25 design parameters of the bicycle, given by Table 1.

Table 1. 25 Design parameters of the Carvallo Whipple model.

Parameter	Symbol	Parameter	Symbol
Wheel base	w	Forward speed	v
trail	c	Steer axis tilt	λ
Rear wheel	R	Front wheel	F
Radius	r_R	Radius	r_F
Mass	m_R	Mass	m_F
Mass moments of inertia	$I_R = \begin{bmatrix} I_{Rxx} & 0 & 0 \\ 0 & I_{Ryy} & 0 \\ 0 & 0 & I_{Rzz} \end{bmatrix}$	Mass moment of inertia	$I_F = \begin{bmatrix} I_{Fxx} & 0 & 0 \\ 0 & I_{Fyy} & 0 \\ 0 & 0 & I_{Fzz} \end{bmatrix}$
Rear frame	B	Front frame	H
Position centre of mass	$Cg_B = \begin{bmatrix} x_B \\ y_B \\ z_B \end{bmatrix}$	Position centre of mass	$Cg_H = \begin{bmatrix} x_H \\ y_H \\ z_H \end{bmatrix}$
Mass	m_B	Mass	m_H
Mass moments of inertia	$I_B = \begin{bmatrix} I_{Bxx} & 0 & I_{Bxz} \\ 0 & I_{Byy} & 0 \\ I_{Bxz} & 0 & I_{Bzz} \end{bmatrix}$	Mass moment of inertia	$I_H = \begin{bmatrix} I_{Hxx} & 0 & I_{Hxz} \\ 0 & I_{Hyy} & 0 \\ I_{Hxz} & 0 & I_{Hzz} \end{bmatrix}$

2.3. Calculation Method

The 25 design parameters are influenced by the bicycle geometrics, the addition of a battery and motor, and the cyclist. The values are determined for the six electric bicycle configurations and a conventional bicycle. The bicycle and cyclist are simplified to geometric shapes (cylinders, torus, cuboids, and spheres) to calculate the inertia tensors in the local centres of gravity. The shapes form a part (cyclist, motor, battery, framework, fork, handlebar, and wheel) and the parts form assemblies (front wheel, rear wheel, front frame, and rear frame). In the case of pedal power assistance, the mass values of the battery is added to the rear frame and the mass values of the motor is added to the front wheel, rear wheel, or rear frame assembly, depending on the motor placement. Table 2 presents an overview of the parts for the seven bicycle configurations.

Table 2. Parts of every assembly for the seven bicycle configurations.

	Bicycle 1	Bicycle 2	Bicycle 3	Bicycle 4	Bicycle 5	Bicycle 6	Bicycle 7
Rear wheel assembly	wheel	wheel	wheel + motor	wheel + motor	wheel	wheel	wheel
Front wheel assembly	wheel + motor	wheel + motor	wheel	wheel	wheel	wheel	wheel
Rear frame assembly	framework + cyclist + battery	framework + cyclist + battery	Framework + cyclist + battery	framework + cyclist + battery	framework + cyclist + battery + motor	framework + cyclist + battery + motor	framework + cyclist
Front frame assembly	handlebar + fork	Handlebar + fork	Handlebar + fork	Handlebar + fork	handlebar+ fork	handlebar+ fork	Handlebar + fork

The inertia tensors are calculated in the centres of gravity of the assemblies. The centre of gravity of the rear frame assembly depends on multiple components (cyclist, motor, battery, and framework) and is calculated afterward. Therefore, the inertia tensor of the shapes are initially calculated in an external, uninfluenced point and for every configuration translated to the centre of gravity of the assembly with a derived formula of the parallel axis theorem (10). The formula is derived as follows.

To translate the inertia tensor of a geometric shape from the local centre of gravity {l} to an external point {o}, the parallel axis theorem is utilized, given by Equation (2).

$$I_o = I_l - m(p_{lo} \, p_{lo}{}^T) + m(p_{lo}{}^T \, p_{lo}) \, I_3 \tag{2}$$

Wherein, I_o is the inertia tensor in {o}, I_l is the inertia tensor in {l}, p_{lo} is the place vector from {o} to {l}, and m is the mass. I_o is translated from the external point {o} to the centre of gravity of a part {c} given by Equation (3) and presented in Figure 4.

$$Ic = Il - m \, p_{lc} \, p_{lc}{}^T + m_{lc}{}^T \, p_{lc} \, I_3 \tag{3}$$

p_{lc} is expressed in function of p_{lo} and p_{co} given by Equation (4).

$$p_{lc} = p_{lo} - p_{co} \tag{4}$$

I_l is expressed in function of I_o given by Equation (5).

$$Ic = Il - m(p_{lo}\,p_{lo}{}^T - p_{lo}p_{co}{}^T - p_{co}p_{lo}{}^T + p_{co}p_{co}{}^T) + m(p_{lo}{}^T p_{lo} - p_{lo}{}^T p_{co} - p_{co}{}^T p_{lo} + p_{co}{}^T p_{co})I_3$$
$$= I_l - m(P_{lo}\,P_{lo}{}^T) + m(P_{lo}{}^T\,P_{lo})\,I_3 - m(-P_{lo}\,P_{co}{}^T - P_{co}\,P_{lo}{}^T + P_{co}\,P_{co}{}^T) + m(-2\,P_{lo}{}^T\,P_{co} + P_{co}{}^T\,P_{co})\,I_3$$
$$= I_o - m(-p_{lo}p_{co}{}^T - p_{co}p_{lo}{}^T + p_{co}p_{co}{}^T) + m(-2p_{lo}{}^T p_{co} + p_{co}{}^T p_{co})I_3$$

(5)

wherein I_c is the inertia tensor in $\{c\}$ and p_{co} is the place vector from $\{o\}$ to $\{c\}$. When the inertia tensors of multiple shapes are translated, I_o is given by (6a) and (6b).

$$I_{o1} = f(I_{l1}, m_1, p_{lo1})$$

(6a)

$$I_{o2} = f(I_{l2}, m_2, p_{lo2})$$

(6b)
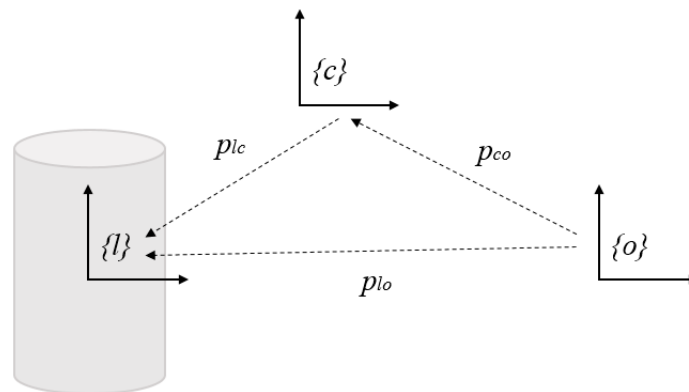
Figure 4. Inertia tensor of a shape is translated to an external point and then to the centre of the gravity of a part.

The mass values of the shapes (i) in $\{o\}$ are summarized to determine the mass values of the part (j) in $\{o\}$, given by (7a) until (7c).

$$I_o{}^{[j]} = \sum I_{oi}{}^{[j]}$$

(7a)

$$m^{[j]} = \sum m_i{}^{[j]}$$

(7b)

$$p_{go}{}^{[j]} = \sum \frac{m_i{}^{[j]}}{m^{[j]}} p_{loi}{}^{[j]}$$

(7c)

wherein p_{go} is the place vector from $\{o\}$ to $\{g\}$ and the centre of mass of part (j).

The inertia tensor of the part is translated from reference frame $\{o\}$ to $\{c\}$, given by Equation (8) and presented in Figure 5.

$$I_c = (fI_{li}, m_i p_{loi}) = \sum I_{li} - m_i\, p_{loi}\, p_{loi}{}^T + m\, p_{loi}{}^T\, p_{loi}\, I_3 - m(-p_{loi}\, p_{co} - p_{co}\, p_{loi}{}^T + p_{co}p_{co}{}^T) + m(-2p_{loi}{}^T p_{co} + p_{co}{}^T p_{co})I_3$$

(8)

p_{loi} is expressed in function of p_{go}, given by (9a) till (9d).
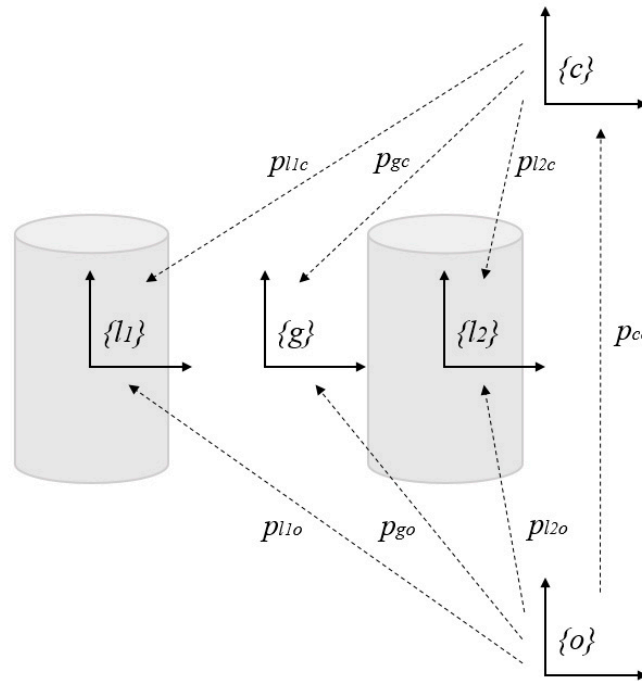
$$m\, p_{go} = \sum_{m_i\, p_{loi}}$$

(9a)

$$\sum_{m_i\, p_{loi}\, p_{co}{}^T} = \left(\sum_{m_i\, p_{loi}} \right) p_{co}{}^T = m\, p_{go}\, p_{co}{}^T$$

(9b)

$$\sum_{m_i\, p_{go}\, p_{loi}{}^T} = p_{co}\left(\sum m_i\, ploi\right) = m\, p_{co}\, p_{go}{}^T \tag{9c}$$

$$\sum_{m_i\, p_{loi}\, p_{co}} = \left(\sum_{m_i\, ploi}\right)^T p_{co} = m\, p_{go}{}^T\, p_{co} \tag{9d}$$

I_c is expressed in function of p_{go}, given by (10).

$$
\begin{aligned}
I_c &= \sum_{I_o} + \sum_{m_i\, p_{loi}\, p_{co}{}^T} + \sum_{m_i\, p_{go}\, p_{loi}{}^T} - \sum_{m_i\, p_{co}\, p_{co}{}^T}\left(-2\sum_{m_i\, p_{loi}\, p_{co}}\right)I_3 + \left(\sum_{m_i\, p_{co}\, p_{co}{}^T}\right)I_3 \\
&= I_o + m\, p_{go}\, p_{co}{}^T + m\, p_{co}\, p_{go}{}^T - m\, p_{co}\, p_{co}{}^T - 2m\, p_{go}{}^T p_{co}I_3 + m\, p_{co}{}^T p_{co}I_3
\end{aligned}
\tag{10}
$$

Figure 5. Inertia tensors of multiple shapes are translated to an external point and then to the centre of gravity of the part.

2.4. Data Acquisition

A market research with five large bicycle stores in Ghent, Belgium ('Fiets! XL Gent','Plum Gent', 'As Adventure Lochristi', 'Het Verzet Deinze,' and 'PDG bikestore Drongen) has led to a list of the 50 most sold city bicycles with and without pedal assistance from the period of 2017 until 2018. The geometrics of the 50 bicycles were measured to determine prototypical dimensions for city bicycles based on the work of Schwab et al. [7]. The results are reported in Table 3. The bicycle parts were not weighted, and the masses were estimated based on literature, material, and volume.

The dimensions of electric and conventional bicycles were compared with t-tests. The geometrics of front and rear wheels without a motor were equal for conventional bicycles and electric bicycles. The geometrics of the rear framework without motor and battery was similar, as electric bicycles with a motor implemented in the front wheel often use a traditional framework. A significant difference was found in the steer stem height, which was positioned 90 mm higher for electric bicycles (with t (48) = 5189, p = 0.001). Consequently, the mass and the center of mass location of the front frame assembly varied due to a difference in steer height. The cyclist posture is more upright and the mass values of the rear frame assembly are different. The dimensions and weight of the motor and battery unit can be found in Table 4.

Table 3. Prototypical dimensions and masses of the seven bicycle configurations.

Bicycle Geometrics	Value Conventional	Electric	Bicycle Geometrics	Value
Stem length	190 mm	270 mm	Steer tube radius	20 mm
Front frame mass	3.20 kg	4.02 kg	Lower mid-tube radius	27.5 mm
Rear framework mass	8.03 kg		Seat tube radius	16 mm
Front wheel mass	3.82 kg		Seat post radius	14 mm
Rear wheel mass	3.80 kg		Rear fork radius	10 mm
Rear hub width	130 mm		Front fork radius	14 mm
Seat post length	210 mm		Bottom bracket height	290 mm
Seat tube angle	69°		Trail	100 mm
Seat tube length	490 mm		Head tube angle	68°
Wheel base	1120 mm		Steer axis tilt	22°
Rear wheel radius	345 mm		Chain stay length	445 mm
Front wheel radius	345 mm		Fork length	470 mm
Handlebar radius	11 mm		Front hub width	100 mm
Steer stem radius	14 mm		Handlebar length	100 mm

Table 4. Standardized dimensions and masses of different motor and battery units.

	Wheel Motor	Mid Drive Motor	Battery Pack in Lower Mid Tube	Battery Pack in Luggage Rack
Weight	2.9 kg	3.1 kg	2.5 kg	2.5 kg
Dimensions [x,y,z]	[160, 100, 160] mm	[200, 180, 150] mm	[330, 90, 90] mm	[370, 120, 80] mm

A bicycle with an adjustable steer stem and seat post is configured according to the standard dimension found for the electric and conventional bicycle. A woman with anthropometric characteristics situated between the 25th and 75th percentiles of the Belgian population is measured and her bicycle posture is captured on the electric and conventional bicycle, which is presented in Table 5. The measurement methods are based on the work of Schwab et al. [7].

Table 5. Anthropometrics of a standardized woman on the electric and conventional bicycle.

Parameter	Value Conventional	Electric	Parameter	Value
Forward lean angle	65°	70°	Upper leg mass	9.71 kg
Weight	64 kg		Upper arm mass	0.99 kg
Length	170 mm		Torso mass	30.93 kg
Hip joint to hip joint	250 mm		Lower leg mass	3.11 kg
Head circumference	540 mm		Lower arm mass	1.13 kg
Lower arm circumference	220 mm		Head mass	3.11 kg
Lower arm length	290 mm		Upper leg length	460 mm
Lower leg circumference	290 mm		Upper leg circumference	500 mm
Lower leg length	460 mm		Upper arm length	260 mm
Torso length	420 mm		Upper arm circumference	240 mm
Chest depth	150 mm		Shoulder to shoulder	390 mm

2.5. Calculations

2.5.1. Inertia Tensors

The electric and conventional bicycles are modelled according to the work of Schwab et al. [7]. The bicycle and cyclist are simplified to geometric shapes fully determined by skeleton points 1 to 33. Point 1 to 31 are defined in the work of Schwab et al. Point 32 is the centre of gravity of the lower mid-tube and point 33 is the centre of gravity of the luggage rack, which is necessary to define the position of the battery unit. All the skeleton points are presented in Figure 6.
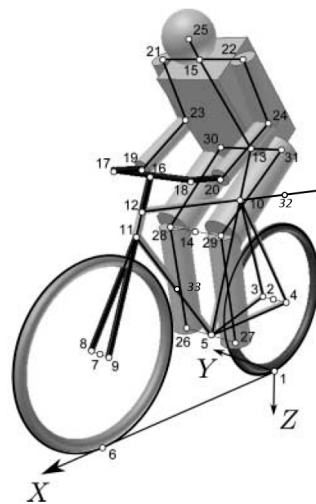
Figure 6. Location of the skeleton points in the bicycle cyclist model.

The inertial tensors of the shapes are calculated in their centres of gravity and are rotated according to their individual position around the *y*-axis and *x*-axis, given by Equation (11).

$$I_l = R(ra)\, I_{cg}\, R(ra)^T \tag{11}$$

where *ra* is the rotation angle around the axis and $R(ra)$ is the rotation matrix around the axis. The rotation matrix around the *y*-axis is given by Equation (12) and the rotation matrix around the *x*-axis is given by Equation (13).

$$R(ra)y = \begin{bmatrix} \cos(ra)_i & 0 & \sin(ra)_i \\ 0 & 1 & 0 \\ -\sin(ra)_i & 0 & \cos(ra)_i \end{bmatrix} \tag{12}$$

$$R(ra)_X = \begin{bmatrix} 1 & 0 & 0 \\ 0 & \cos(ra)_i & -\sin(ra)_i 0 \\ 0 & \sin(ra)_i & \cos(ra)_i \end{bmatrix} \tag{13}$$

The rear frame assembly considers the following parts: the rear framework (I_{Bb}), the cyclist in the electric posture ($I_{Bc(electric)}$), or in the conventional one ($I_{Bc(conventionall)}$) and optionally a mid-drive motor ($I_{M(crank)}$) and battery unit in the lower mid-tube ($I_{A(tube)}$) or on the luggage rack ($I_{A(luggage)}$). Table 6 presents the different configurations. The inertia tensors from the shapes that form the parts are translated with the parallel axis theorem to the origin of the coordinate system (skeleton point 1), given by Equation (2), and are summed to determine the inertia tensors of the parts in skeleton point 1. The centre of gravity of the parts are determined and given by Figure 7C. The centre of gravity of the rear frame assembly of every configuration is calculated (Cg_B), given by Equation (4) and the derived formula of the parallel axis theorem is utilized to translate the inertia matrix in skeleton point 1 to Cg_B, given by Formula (10).

Table 6. Inertia tensors of the rear frame assembly.

	Bicycle 1	Bicycle 2	Bicycle 3	Bicycle 4	Bicycle 5	Bicycle 6	Bicycle 7
Rear frame assembly	$I_{Bb} +$ $I_{Bc(electric)} +$ $I_{A(luggage)}$	$I_{Bb} +$ $I_{Bc(electric)} +$ $I_{A(tube)}$	$I_{Bb} +$ $I_{Bc(electric)} +$ $I_{A(luggage)}$	$I_{Bb} +$ $I_{Bc(electric)} +$ $I_{A(tube)}$	$I_{Bb} + I_{Bc(electric)}$ $+ I_{M(crank)} + I_{A(luggage)}$	$I_{Bb} + I_{Bc(electric)}$ $+ I_{M(crank)}$ $+ I_{A(tube)}$	$I_{Bb} +$ $I_{Bc(conventionall)}$
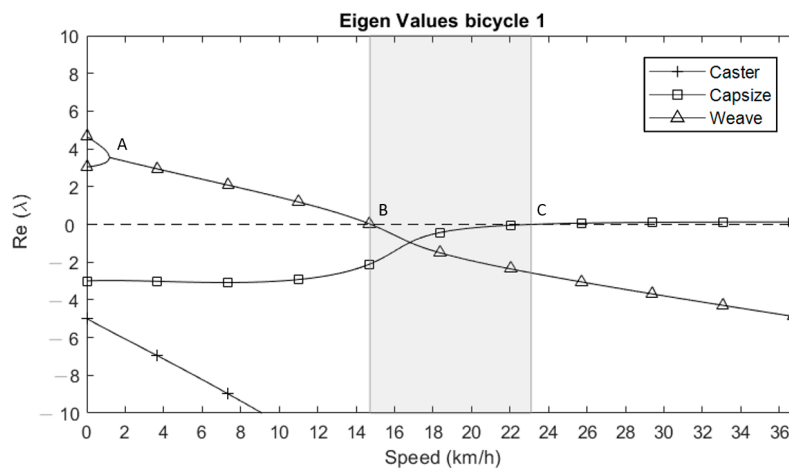
Figure 7. Stability behaviour of bicycle configuration 1.

As the front frame is fully defined by the handlebar and fork and it has only two configurations: one for the electric bicycle, which is a bit higher and heavier and one for the conventional bicycle. The inertia tensor is directly determined in the centre of gravity of the assembly.

The front wheel and rear wheel assembly are fully defined by the wheel and, optionally, an electromotor with the same centre of gravity. Consequently, the inertia tensor is directly determined in the centres of gravity of the assemblies.

2.5.2. Eigenvalues

The eigenvalues of the linearized equation of the Carvallo Whipple model (1) are calculated to evaluate the self-stability of the seven bicycle configurations [1,2]. Three modes determine the stability of the bicycle: capsize, weave, and caster. In the capsize mode, the bicycle leans into a spiral path until it ultimately keels over. In general, the capsize is stable at low speeds, and becomes less stable as speed increases. In the weave mode, the bicycle presents an oscillation between the leaning left and steering right and vice versa. Weave is generally unstable at low speeds, and becomes less pronounced as speed increases until it is no longer unstable. Weave is an oscillation around the heading of the bicycle, while caster describes a motion around the steering axis. The caster mode is comparable with the mechanism of a caster wheel on a shopping cart and is overall stable while the capsize and weave mode determine the stability range of the bicycle [7].

3. Results

All bicycle configuration present similar graphs. Figure 7 addresses an example of the eigenvalues, namely from bicycle configuration 1. From 0 km/h till point A, four eigenvalues are found: two positive ones from the weave mode corresponding to a falling motion and two negative ones from the capsize and caster mode corresponding to a righting motion. The weave mode dominates and, without any rider corrections, the bicycle falls over as an unstabilized inverted pendulum. At point A, the two positive eigenvalues form a complex conjugate pair and the steering perturbation lead to an oscillatory weave motion. From point A until point B, the bicycle is less stable by the decreasing eigenvalue of the weave mode. From point B until point C, all the eigenvalues are negative and the corrective actions of the bicycle are large enough to prevent the bicycle from falling and small enough to not exhibit overcorrection. The bicycle is self-stable without any actions of the cyclist.

As only the capsize and weave mode are significant for bicycle stability, the seven bicycle configurations are compared based on these values. Table 7 present the cycling speed of (i) the transition of the inverted pendulum motion to the oscillatory weave motion in point A, (ii) the start of the self-stable mode in point B, and (iii) the end of the self-stable mode in point C. Initially, the bicycles present the motion of an unstabilized inverted pendulum. For bicycle 1 and 2, it reaches up to 1.25 km/h.

For bicycle 3 until 7, it reaches up to 1.40 km/h. After this point, the bicycles get increasingly more stable and presents an escalating weave oscillation. For bicycle 1 and 2, it reaches up to 14.72 km/h, for bicycle 3 to 14.64 km/h, for bicycle 4 to 14.57 km/h, for bicycle 5 and 6 to 14.50 km/h, and for bicycle 7 to 14.28 km/h. Subsequently, the self-stable mode starts and reaches up to 23.09 km/h for bicycle 1, to 23.68 km/h for bicycle 2, to 22.07 km/h for bicycle 3, to 22.66 km/h for bicycle 4, to 22.44 km/h for bicycle 5, to 23.10 km/h for bicycle 6, and to 22 km/h for bicycle 7. From point A to B, the bicycle is easy to stabilize. This semi-stable range is 13.47 km/h for bicycle 1 and 2, 13.24 km/h for bicycle 3, 13.17 km/h for bicycle 4, 13.1 km/h for bicycle 5 and 6, and 12.88 km/h for bicycle 7. From point B to C, the bicycle is self-stable. The self-stable range is 8.37 km/h for bicycle 1, 8.96 km/h for bicycle 2, 7.43 km/h for bicycle 3, 8.09 km/h for bicycle 4, 7.94 km/h for bicycle 5, 8.6 km/h for bicycle 6, and 7.72 km/h for bicycle 7. The sum of both ranges counts 21.84 km/h for bicycle 1, 22.43 km/h for bicycle 2, 20.67 km/h for bicycle 3, 21.26 km/h for bicycle 4, 21.04 km/h for bicycle 5, 21.70 km/h for bicycle 6, and 20.6 km/h for bicycle 7.

Table 7. Key points and ranges of the stability behaviour of every bicycle configuration.

Velocity [km/h]	Bicycle 1	Bicycle 2	Bicycle 3	Bicycle 4	Bicycle 5	Bicycle 6	Bicycle 7
Point A	1.25	1.25	1.40	1.40	1.40	1.40	1.40
Point B	14.72	14.72	14.64	14.57	14.50	14.50	14.28
Point C	23.09	23.68	22.07	22.66	22.44	23.10	22.00
Semi stable range	13.47	13.47	13.24	13.17	13.1	13.1	12.88
Self-stable range	8.37	8.96	7.43	8.09	7.94	8.6	7.72
Semi and Self-stable range	21.84	22.43	20.67	21.26	21.04	21.7	20.6

Figure 8 presents the deviation from the mean for every bicycle configuration for point A, B, C and for the semi-stable range, self-stable range, and the sum of both. The horizontal lines correspond to the mean and two times the standard deviation. When comparing the points, the highest difference is found for bicycle 7 in point B. However, no significant differences are found since all the values are within two times the standard deviation.
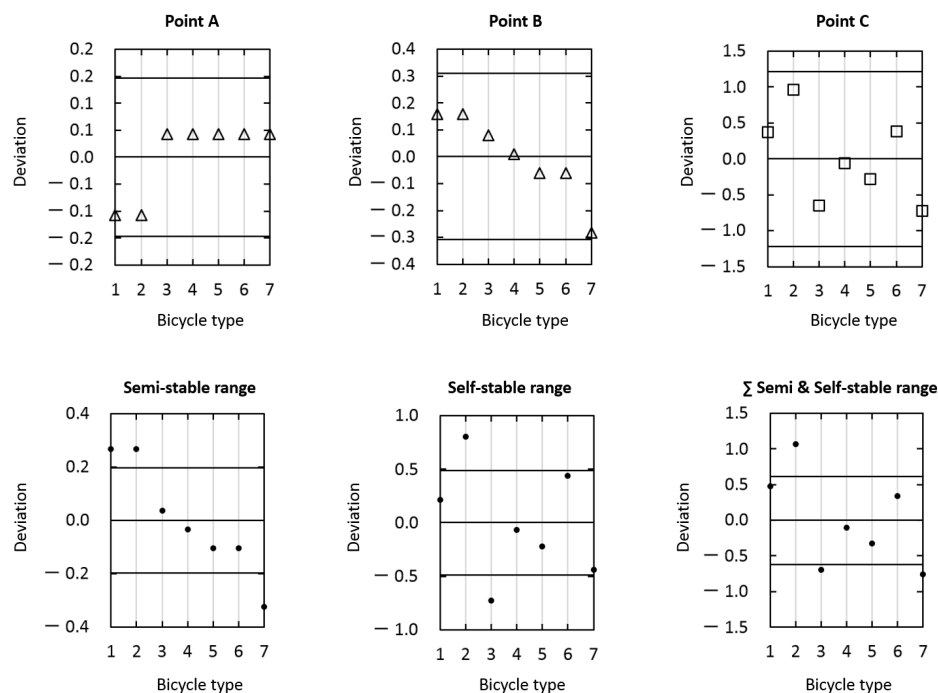
Figure 8. Deviation from the mean for every bicycle configuration for the six key points and ranges.

When addressing the ranges, some significant differences are found. The semi-stable range is significantly higher for bicycle configuration 1 and 2 and smaller for bicycle configuration 7. The self-stable range is significantly higher for bicycle configuration 2 and smaller for bicycle configuration 3. When comparing the whole range when the bicycle is easy to stabilize, bicycle 2 performs significantly better than the other configurations. Bicycle configuration 3 and 7 perform significantly less.

4. Discussion

Literature shows that a forward leaned rider with stretched arms and hands on the handlebar have little influence on the self-stability behaviour of a bicycle while an upright rider position with flexed arms and hands on the handlebar changes the open-loop dynamics drastically, which results in a decreased self-stability [7]. Since the forward lean angle on the conventional bicycle is smaller (65° versus 70°) than on the electric one, a better self-stable behaviour is expected for the conventional bicycle. On the other hand, the difference in the forward lean is the result of a difference in the front frame assembly. Collins concluded that the centre of gravity of the front frame assemble should be 9 cm in front of the steering axis, which is measured perpendicularly on the steer tube [12]. The centre of gravity of the front frame assembly of the electric bicycle is closer to the optimum described by Cornell, which results in an enhanced self-stable behaviour of the electric bicycle. Since both systems counteract, only marginal differences are found between the conventional and electric bicycles. The self-stable mode of the conventional bicycle starts at a lower speed than the electric bicycles. Additionally, the complex conjugate pair is formed early, which causes a significantly smaller semi-stable range than the electric bicycles. The self-stable range is relatively small, even though the electric bicycle with the motor in the rear wheel and the battery pack in the luggage rack (configuration 3) performs worse. When considering the whole period, the bicycle is easy to stabilize. The conventional bicycle and the electric bicycle with the motor in the rear wheel and the battery pack in the luggage rack perform worse.

Significant differences are found between the six electric bicycle configurations. Most notably, the semi-stable range is significantly higher for the electric bicycles with a motor in the front wheel. Bottomley described the "gyroscopic self-stabilization" of a bicycle in 1868. The gyroscopic effect of a spinning front wheel increases the stability [13]. Currently, the idea is universally accepted in literature [14]. Addressing electric bicycles, the front wheel motor adds weight to the front wheel assembly, which increases the self-stabilization effect. When taking the self-stable range into account, the electric bicycle with a front wheel motor and a battery located in the lower mid-tube performed the best. Furthermore, this effect is observed for every bicycle configuration. When a battery is located in the lower mid-tube, the self-stable range is higher than when the battery is located in the luggage rack. Jones discussed that the gyroscopic effect is only relevant for a light riderless bike, whereas a heavier cyclist overpowers the effect [4]. Similar to the influence of the cyclist's posture discussed by Schwab et al. [7], the differences could be assigned to the lower location of the centre of mass of the rear frame assembly due to the lower battery placement.

Knowledge about the stability behaviour of common bicycles can improve bicycle design to increase the level of comfort of the cyclist. A low A and B value and a high C value is preferred to minimize the counteractions of the user and increase the bicycle stability. The study showed that motor and battery placement significantly influence the stability behaviour. However, it should be noted that cyclist weight and posture are equally important. For future work, different types of cyclists should be taken into account.

5. Conclusions

Significant differences are found in the self-stable and semi-stable range between electric and conventional bicycles. The more upright posture on an electric bicycle decreases the self-stable range, while the higher steer stem improves it. In general, this leads to a lower self-stable and semi-stable range for conventional bicycles. Electric bicycles with a motor implemented in the front wheel perform best, as the extra weight of the motor enhances the gyroscopic self-stabilization of the front wheel.

Furthermore, a lower centre of mass of the rear frame assembly positively influences the stability behaviour. Therefore, a motor in the lower mid tube is preferred over a higher located motor in the luggage rack.

References

1. Carvallo, E. *Théorie du Mouvement du Monocycle et de la Bicyclette*; Gauthier-Villars: Paris, France, 1899.
2. Whipple, F.J.W. The stability of the motion of a bicycle. *Quart. J. Pure Appl. Math* **1899**, *30*, 312–348.
3. Meijaard, P.; Papadopoulos, J.M.; Ruina, A.; Schwab, A.L. Linearized dynamics equations for the balance and steer of a bicycle: A benchmark and review. *Proc. R. Soc. A* **2007**, *463*, 1955–1982. [CrossRef]
4. Jones, D.E.H. The stability of the bicycle. *Phys. Today* **1970**, *23*, 34–40, (reprinted in September 2006). [CrossRef]
5. Stevens, D. Stability and Handling Characteristics of Bicycles. Bachelor' Thesis, University of New South Wales, Wales, UK, 2009.
6. Weir, D.H.; Zellner, J.W. Experimental investigation of the transient behavior of motorcycles. *SAE Trans.* **1979**, *88*, 962–978.
7. Schwab, A.L.; Meijaard, J.P.; Kooijman, J.D.G. Lateral dynamics of a bicycle with a passive rider model: Stability and controllability. *Veh. Syst. Dyn.* **2012**, *50*, 1209–1224. [CrossRef]
8. Williams, T.A. Influence of Frame Stifness and Rider Position on Bicycle Dynamics: An Analytical Study. Master's Thesis, University of Wisconsin-Milwaukee, Milwaukee, WI, USA, 2015.
9. Oortwijnon, J. Europe's E-Bike Imports Indicate Market Size. *Bike Eur.* **2013**. Available online: https://www.bike-eu.com/sales-trends/nieuws/2013/08/europes-e-bike-imports-indicate-market-size-10110166?vakmedianet-approve-cookies=1&_ga=2.237040071.691246130.1597627420-725384798.1597627420 (accessed on 23 July 2020).
10. Schepers, J.P.E.; Fishman, P.; den Hertog, K.; Klein, W.; Schwab, A. The safety of electrically assisted bicycles compared to classic bicycles. *Accid. Anal. Prev.* **2014**, *73*, 174–180. [CrossRef] [PubMed]
11. Twisk, D.A.M.; Platteel, S.; Lovegrove, G.R. An experiment on rider stability while mounting: Comparing middle-aged and elderly cyclists on pedelecs and conventional bicycles. *Accid. Anal. Prev.* **2017**, *105*, 109–116. [CrossRef] [PubMed]
12. Collins, R.N. A Mathematical Analysis of the Stability of Two Wheeled Vehicles. Ph.D. Thesis, University of Wisconsin, Madison, WI, USA, 1963.
13. Bottomley, J.F. Balancing and no hands. In *The Velocipede, Its Past, Its Present & Its Future*; Simpkin, Marshall & Co.: London, UK, 1868; pp. 14, 38–47.
14. Meijaard, J.P.; Papadopoulos, J.M.; Ruina, A.; Schwab, A.L. Historical review of thoughts on bicycle self-stability. *Sci. Mag.* **2011**, 1–41.